Transient simulation of electron emission from quantum-wire structures

S. Briggs and J. P. Leburton
Beckman Institute for Advanced Science and Technology, Department of Electrical and Computer Engineeering, University of Illinois at Urbana-Champaign, Urbana, Illinois 61801
(Received 30 April 1990; revised manuscript received 30 July 1990)

We model a GaAs quasi-one-dimensional quantum wire in an applied longitudinal field and focus on mechanisms of electron emission leading to real-space transfer from the wire. The Monte Carlo simulation assumes an initial electron distribution in the wire and calculates the time required for electrons to undergo nonequivalent intervalley scattering to three-dimensional states. The model includes multiple subbands, polar optic and acoustic phonons, intervalley scattering, and band-structure nonparabolicity. Results have been obtained for different confinement conditions as well as different temperatures. We find that the required time is a very strong function of the longitudinal field and ranges from 4 ns down to 1 ps for fields in the range of 100 V/cm to 8 kV/cm. The corresponding distances in the wire vary from 130 μm down to the submicrometer range.

I. INTRODUCTION

The physics and fabrication of quasi-one-dimensional (1D) artificial structures have experienced rapid progress in the past few years.[1-9] While early confined systems were limited to the observation of quantum effects at low temperature, 1D effects are now observable well above liquid-helium temperature. Quantum wires with carrier confinement below 1000 Å have recently been achieved and quantum features in the transconductance of 1D field-effect devices have been reported at 77 K.[7] Meanwhile, new approaches to fabricate quantum structures with two degrees of confinement by direct growth on vicinal GaAs substrates have demonstrated the feasibility of quantum-wire based lasers,[8,9] which raises issues concerning the dynamics and dissipation of nonequilibrium carriers in 1D systems. Above 77 K, transport is essentially limited by phonon scattering which is a strong impediment to the observation of quantum interference effects. Also, high-temperature operation is desirable and the interesting aspect of 1D transport is the reduction of transverse degrees of freedom which tends to limit scattering to forward and backward events.[10] Under these conditions, thermal effects become determinant and 1D transport is described in terms of a semiclassical Boltzmann formalism. Theoretical investigations of the electronic properties of semiconductor wire structures have been accomplished including calculation of the dominant scattering mechanisms[11-14] and transport simulations.[15-17]

One serious unresolved issue is carrier emission from the quantum wire, since at sufficiently high electric fields, the carriers gain enough energy to overcome the confining barrier.[15] The escape mechanisms depend on the wire configuration and include real-space transfer effects[18] such as emission from a quantum-well confining potential or drift away from a heterojunction triangular confining potential. Carrier losses due to scattering include intravalley as well as intervalley phonon scattering to 3D states. If the losses due to these mechanisms are significant, either in terms of electron lifetimes in the wire or mean paths in the wire, then the whole concept of an infinitely long, semiclassical quantum wire is invalid. To date, no work has addressed this question.

II. MODEL

We simulate electron transport with a Monte Carlo technique which is based on a model consisting of a GaAs-$Al_xGa_{1-x}As$ quantum well (QW) and a perpendicular gate electrode with a triangular electrostatic potential. The model includes seven electronic subbands. Figure 1 shows this configuration, which is similar to the V-shaped-groove quantum-wire field-effect transistor[1] (VFET) or the modulation doped GaAs-$Al_xGa_{1-x}As$ wire structures fabricated using ion-beam-assisted etching.[6] The V-shaped-groove wire, characterized by a quantum well in the y direction and a triangular potential in the z direction, offers, in principle, the largest degree of confinement that can be controlled by external transverse electric fields (gate fields) F_z. Although different confinement configurations may be considered, the conclusions obtained with this configuration can be generalized to any kind of geometrical confinement.

For the y direction we calculate wave functions in the infinite square-well approximation while in the z direction we perform a variational calculation with exponentially damped polynomials as the trial wave functions. We compute the first three y and z wave functions and combine them to obtain nine wave functions. Then, the total wave functions Ψ are given by

$$\Psi_{i,j}(x)=e^{-ik_x x}\left[\frac{2}{L_y}\right]^{1/2}\sin\left[\frac{i\pi y}{L_y}\right] \times e^{-\zeta_j z}\sum_{n=1}^{n=j} c_{n,j}z^n, \quad i=1,2,3, \quad j=1,2,3 \tag{1}$$

where ζ_j and $c_{n,j}$ are determined by a variational calculation as well as the corresponding energy E_j; we also have

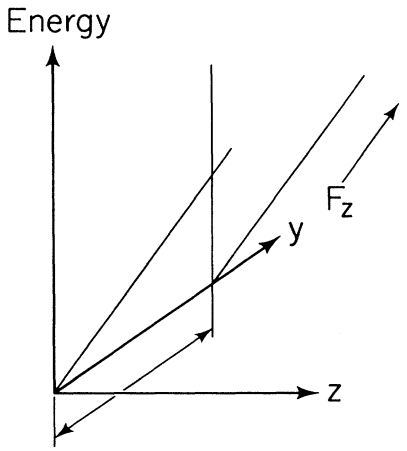

FIG. 1. Idealized structure used in the simulation. Confinement in the y direction is due to a quantum well of width L_y. F_z is the applied field in the z direction which gives rise to a triangular well.

assumed free electrons (plane waves) in the x direction. The corresponding energies of the subband bottoms are given by

$$E_{i,j}=\frac{(\hbar\pi i)^2}{2m^*L_y^2}+E_j, \quad i=1,2,3, \quad j=1,2,3 \ . \tag{2}$$

These approximations are good if the energy level lies deep in the well. The higher y levels should be spaced more closely as they approach the top of the QW and the z levels spaced more closely as screening flattens out the triangular potential. The $y=2, z=3$ and $y=3, z=3$ states are omitted because of memory constraints in the Monte Carlo code. For most confinement conditions of interest, these two levels are above the edge of the GaAs-$Al_xGa_{1-x}As$ barrier and can be neglected. Although the lowest energy level is clearly $E_{1,1}$, the ordering of the higher subbands depends on the confinement conditions. To avoid confusion, the subbands will be numbered with a single subscript ν, which will range in order of increasing energy from 1 for the lowest subband to 7 for the highest subband. The y and z quantum numbers will, in general, not be used.

Because of the relatively high energy transport considered in this simulation, nonparabolic effects in the band structure are important and have been included in the model using the Kane approximation[19] with a nonparabolicity factor $\alpha=0.67\ \text{eV}^{-1}$. Then, the relation between $E(k_x)$, the electron energy in the subband, and k_x, the longitudinal wave factor, is given by

$$\frac{\hbar^2}{2m^*}(k_\nu^2+k_x^2)=[E(k_x)+E_\nu]\{1+\alpha[E(k_x)+E_\nu]\}$$
$$=E_T(\tilde{k})[1+\alpha E_T(\tilde{k})] \tag{3a}$$

with

$$k_\nu^2=\frac{2m^*}{\hbar^2}E_\nu(1+\alpha E_\nu) \ , \tag{3b}$$

$$k_x^2=\frac{2m^*}{\hbar^2}E(k_x)\{1+\alpha[E(k_x)+2E_\nu]\} \ , \tag{3c}$$

and

$$\tilde{k}=(k_x,k_\nu) \ . \tag{3d}$$

E_ν is the energy at the bottom of the subband; here we have defined the total energy relative to the quantum-well bottom as $E_T(\tilde{k})=E_\nu+E(k_x)$. We express k_ν in terms of the energy and do not attempt to define k_y and k_z because only the magnitude of k_y can be determined and k_z is not even a constant of motion. In addition, it is important to note that $\tilde{k}$ is defined as an ordered pair rather than a vector, the reason being it does not transform as a vector (i.e., it is not closed under addition or scalar multiplication). The $E(k_x)$ relation is now a function of not only the energy relative to the subband bottom but also the energy of the subband relative to the quantum well. The density of states is also now a function of both E_ν and $E(k_x)$.

For the satellite valleys, since the effective masses are large, the level splitting brought about by the confinement will be small; therefore we assume that only 3D states exist in the X and L valleys. We consider polar optic, acoustic, and intervalley phonon scattering mechanisms. At present, the 1D Monte Carlo code is not interfaced to a 3D transport code for electrons in the satellite valleys and our model does not include any mechanism for electron injection into the wire. Due to this approximation, our results are limited to the transient case where all electrons are in the wire at time t equals zero; we study the time evolution of the system as electrons escape to 3D states.

III. SCATTERING RATES

In general, the transition rate from a wave vector $\mathbf{k}$ to $\mathbf{k}'$ is given by Fermi's golden rule[20]

$$W(\mathbf{k},\mathbf{k}')=\frac{2\pi}{\hbar}|H_{fi}|^2\delta(E_{\text{final}}-E_{\text{initial}}) \ , \tag{4}$$

where H_{fi} is the matrix element of the perturbing potential H between the initial and final states. The transition rate is modified due to nonparabolic effects in the conduction band, which introduces a term $G(\mathbf{k},\mathbf{k}')$. This term represents the overlap integral between the periodic parts of the Bloch functions at $\mathbf{k}$ and $\mathbf{k}'$ summed over the doubly degenerate final spin states and averaged over the initial spin states. For 3D cases, this is equal to[21]

$$G(\mathbf{k},\mathbf{k}')=(a_\mathbf{k}a_{\mathbf{k}'}+c_\mathbf{k}c_{\mathbf{k}'}\cos\beta)^2 \ , \tag{5a}$$

with

$$a_\mathbf{k}=\left[\frac{1+\alpha E_T(\mathbf{k})}{1+2\alpha E_T(\mathbf{k})}\right]^{1/2},$$
$$c_\mathbf{k}=\left[\frac{\alpha E_T(\mathbf{k})}{1+2\alpha E_T(\mathbf{k})}\right]^{1/2}, \tag{5b}$$

and β the angle between $\mathbf{k}$ and $\mathbf{k}'$ [then $\cos\beta=(k_xk_x'+k_yk_y'+k_zk_z')/|\mathbf{k}||\mathbf{k}'|$]. In 1D systems the en-

ergy quantization replaces $\mathbf{k}$ by $\tilde{k}$ in which case only k_x and k_ν are known whereas k_y and k_z are undetermined; this makes β undetermined. To overcome this difficulty, we average $\cos\beta$ over all possible values of k_y, k_z, k_y', and k_z' subject to the constraint $k_\nu^2=k_y^2+k_z^2$ and similarly for k_ν'. Although it may be argued that k_y is a good quantum number with discrete values, fixing k_y fixes k_z as well; however, this k_z value does not correspond to any physical quantity. The $\cos\beta$ term is derived assuming plane waves and it is not clear that either k_y or k_z are the corresponding quantities in the 1D form of $\cos\beta$. In addition, using explicit values for k_y and k_z still requires an averaging process, since the signs of k_y and k_z are undetermined. Rather than making these assumptions, we simply average over k_z and k_y as well. This method of determining β is certainly an approximation to calculating the overlap between initial and final Bloch functions; however, this seems the most reasonable approach given the small magnitude of $c_{\tilde{k}}$. β is thus obtained as a function of k_x, k_x', k_ν, and k_ν', which are all known quantities. With this assumption, $G(\tilde{k},\tilde{k}')$ becomes

$$G(\tilde{k},\tilde{k}')=(a_{\tilde{k}}a_{\tilde{k}'})^2+2a_{\tilde{k}}a_{\tilde{k}'}c_{\tilde{k}}c_{\tilde{k}'}\times\frac{k_xk_x'}{(k_x^2+k_\nu^2)^{1/2}(k_x'^2+k_\nu'^2)^{1/2}}+(c_{\tilde{k}}c_{\tilde{k}'})^2\frac{(k_x^2k_x'^2+\frac{1}{2}k_\nu^2k_\nu'^2)}{(k_x^2+k_\nu^2)(k_x'^2+k_\nu'^2)} \tag{6a}$$

for intersubband transitions and

$$G(\tilde{k},\tilde{k}')=(a_{\tilde{k}}a_{\tilde{k}'})^2+2a_{\tilde{k}}a_{\tilde{k}'}c_{\tilde{k}}c_{\tilde{k}'}\times\frac{k_xk_x'+k_\nu^2}{(k_x^2+k_\nu^2)^{1/2}(k_x'^2+k_\nu'^2)^{1/2}}+(c_{\tilde{k}}c_{\tilde{k}'})^2\frac{(k_xk_x'+k_\nu^2)^2}{(k_x^2+k_\nu^2)(k_x'^2+k_\nu'^2)} \tag{6b}$$

for intrasubband transitions.

Currently, we consider polar-optic-phonon (POP) and inelastic-acoustic-phonon scattering for 1D states within the Γ valley. In addition, we consider intervalley scattering from 1D states in the Γ valley to 3D states in the X or L valleys. For POP or acoustic phonons, the transition probabilites from an electron state k_x in initial subband ν to a state k_x' in final subband μ are calculated according to Fermi's golden rule as

$$W_{\nu,\mu}(k_x,k_x')=\frac{2\pi}{\hbar}\delta_{k_x-k_x',q_x}G(\tilde{k},\tilde{k}')\times\int_{-\infty}^{+\infty}\int_{-\infty}^{+\infty}dq_ydq_z|M_{3\mathrm{D},\nu,\mu}(q_x,q_y,q_z)|^2\times(N_q+\tfrac{1}{2}\pm\tfrac{1}{2})\delta([E_\nu+E(k_x)]-[E_\mu+E(k_x')]\pm\hbar\omega_q), \tag{7}$$

where q_x is the longitudinal and q_y, and q_z the transverse phonon wave vectors, respectively. N_q is the phonon occupation number with the plus or minus sign corresponding to phonon emission or absorption. The double integral over q_y and q_z represents the calculation of the 1D matrix elements $M_{1\mathrm{D},\nu,\mu}(q_x)$ from the 3D matrix elements.[15] Here we consider only bulk (i.e., 3D) phonon modes and neglect 1D and surface modes. This does not introduce significant error as long as the confinement is not excessively high, i.e., less than 50 Å.[22] The POP dispersion relation is assumed to be a constant, which makes N_q and the energy conservation δ function independent of q; therefore they can be factored out of the double integral. However, the nonconstant dispersion relation for acoustic phonons makes computation of the integral considerably more complex. The numerical integration routine has q_x as an input parameter, which we vary to obtain 1D matrix elements. For acoustic phonons, we evaluate the integral for q_x in the range $7\times10^4<q_x<1.5\times10^7$ cm^{-1}. The acoustic-phonon transition probabilities are essentially independent of q_x for smaller values, while 1.5×10^7 cm^{-1} is the largest possible momentum exchange. For POP transitions, the integral is evaluated for $1<q_x<1\times10^7$ cm^{-1}.

The δ_k term in Eq. (7) represents conservation of longitudinal momentum with the plus or minus sign corresponding to forward or backward phonon scattering, respectively, and is used to select a value for q_x and the corresponding matrix element. Scattering rates are computed by integrating the transition probabilities over the final electron k states. The total scattering rate for POP's or acoustic phonons from initial state k_x in subband ν is then given by

$$\lambda_\nu(k_x)=\sum_{\mu=1}^{7}\frac{2\pi}{\hbar}|M_{1\mathrm{D},\nu,\mu}(q_x)|^2\delta_{k_x-k_x',q_x}\times\frac{m}{\hbar^2}\frac{(1+2\alpha E_T')}{k_x'}G(\tilde{k},\tilde{k}') \tag{8a}$$

with

$$|k_x'|=\left[\frac{2m^*}{\hbar^2}[E_T'(1+\alpha E_T')-E_\mu(1+\alpha E_\mu)]\right]^{1/2} \tag{8b}$$

and

$$E_T'=E_T\pm\hbar\omega_{\mathrm{LO}}\ . \tag{8c}$$

Equations (8b) and (8c) represent conservation of energy and determine the final k state and the factor $2\alpha E_T'$ in Eq. (8a) is due to nonparabolicity in the final density of states. For each 1D subband, conservation of energy gives four possible final states corresponding to forward or backward emission or absorption.

A constant broadening factor was used to account for quantum corrections to the final density of states. Because of the divergence in the classical density of states at the bottom of a subband, we consider quantum correlations between scattering events and neglect other intracollisional effects such as the influence of the field or phonon lifetime. The density-of-states broadening was selected by fitting the scattering rates from Fermi's golden rule to the imaginary part of the polaron self-energy obtained from a self-consistent solution to the Fock ap-

proximation and was found to be equal to 2.5 meV at 300 K and 1.6 meV at 77 K.[23] A similar broadening factor was also used for acoustic-phonon and intervalley scattering.

For intervalley scattering, the transition rate between state k_x in subband ν of the Γ valley and state k' in the X or L valley is given by

$$W_{\nu,X,L}(k_x,\mathbf{k}') = \frac{2\pi}{\hbar}\delta_{k_x-k_x',q_x} G(\tilde{k},\mathbf{k}') \times \int_{-\infty}^{+\infty}\int_{-\infty}^{+\infty} dq_y dq_z |M_{3D,\nu,X,L}(q_x,q_y,q_z)|^2 \times (N_q+\tfrac{1}{2}\pm\tfrac{1}{2})\delta[E_T(\tilde{k})-E_{X,L}(\mathbf{k}') \pm\hbar\omega_{X,L}] , \quad (9)$$

where $E_{X,L}(\mathbf{k}')$ is the total energy of the final state relative to the bottom of the quantum well (i.e., the bottom of the Γ valley) and $\hbar\omega_{X,L}$ the intervalley phonon energy. Again, we assume 3D modes and a constant dispersion relation which allows us to factor N_q and the energy-conservation δ function out of the integral. In addition, the form of the matrix element allows the integral to be separated into two independent single integrals over q_y and q_z without any q_x dependence. Then, $S_{\nu,L}(k_x)$, the total rate to a specific L valley, is given by

$$S_{\nu,L}(k_x) = \frac{2\pi}{\hbar}|M_{1D,\nu}(q_x)|^2\delta_{k_x-k_x',q_x}(N_q+\tfrac{1}{2}\pm\tfrac{1}{2}) \times k'\frac{m_L^*}{\hbar^2}(1+2\alpha_L E_L) , \quad (10a)$$

with the final k state $\mathbf{k}'$ given by

$$|\mathbf{k}'| = \left[\frac{2m_L^*}{\hbar^2}E_L(1+\alpha_L E_L)\right]^{1/2} , \quad (10b)$$

and the final energy relative to the bottom of the L valley,

$$E_L = [E_\nu + E(k_x)] - \Delta_L \pm \hbar\omega_L . \quad (10c)$$

Δ_L is the energy difference between L and Γ. A similar expression holds for $S_{\nu,X}(k_x)$. Then, the total intervalley scattering rate is given by

$$\lambda_\nu(k_x) = 3S_{\nu,X}(k_x) + 4S_{\nu,L}(k_x) , \quad (10d)$$

with the factors of 3 and 4 accounting for the number of satellite valleys.

The scattering rates are shown in Fig. 2. For the sake of clarity, only the bottom two subbands are shown with a being the lowest subband and b the first excited state. The threshold for intervalley absorption to the L valley occurs at 262 meV and the onset of emission to the L valley begins at 318 meV. Absorption to the X valley starts at 450 meV and emission to that valley occurs above 510 meV. The rates for POP and acoustic phonons show a large number of peaks, each peak being proportional to the density of final states and corresponding to an emission or absorption to the bottom of a subband (the peaks at higher energy represent scattering to subbands not shown in the figure). These peaks make the velocity and distribution functions sensitive to the energy separation between subbands, particularly the first and second subbands. Although the scattering rates for POP and acoustic phonons are different for the different subbands, we can see that the rate for intervalley scattering is independent of the initial subband.

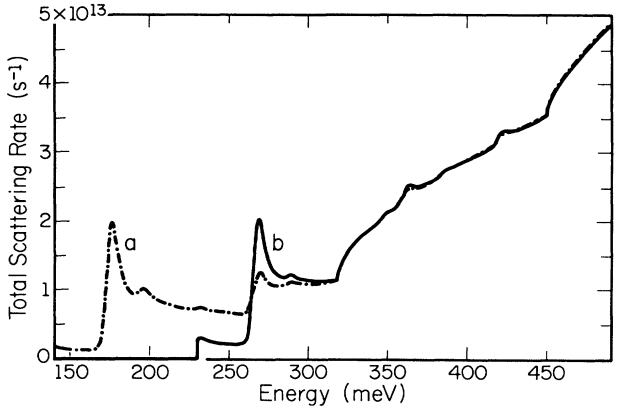

FIG. 2. Scattering rates for a quantum-wire structure including POP, acoustic, and intervalley phonons. The confinement conditions are $L_y = 135$ Å, $F_z = 120$ kV/cm, and $T = 300$ K. Although the rates include transitions between all seven subbands, only the lowest two subbands are shown for the sake of clarity. The peaks in the rates are due to POP scattering to the bottom of a subband. Clearly visible are the thresholds for phonon absorption to the L valley at 262 meV, emission to the L valley at 318 meV, and absorption to X valley at 450 meV. The emission threshold to the X valley at 510 meV is not on the graph, but is included in the simulation.

IV. MONTE CARLO SIMULATION

Because of the large number of peaks in the rates, normal methods of computing free flight times are inefficient. Using constant or piecewise constant scattering rates[24,25] with self-scattering would have introduced a very large percentage of self-scattering events. Instead, a direct integration method was used. For a given subband ν, if r is a uniformly distributed random number on [0,1], then

$$-\ln r = \int_0^t \lambda_\nu[k_\nu(t')]dt' , \quad (11)$$

where t is the time of the free flight, $k_\nu(t)$ is the momentum as a function of time in subband ν, and $\lambda_\nu(k_\nu)$ is the scattering rate as a function of momentum for that subband. In 3D simulations it is virtually impossible to store $\mathbf{k}(E)$ in tabular form because of the large number of possible k values. In 1D systems, there is only one scalar k_ν value for each energy and each ν (tabulated earlier by the program), therefore $k(E)$ is simply a lookup function. Moreover, in 3D, dt is a complicated function of k, involving squares and square-root computations, which typically prohibits direct integration algorithms in Monte Carlo techniques. For 1D systems, however, direct integration compares favorably with other methods.

For a given initial electron energy and subband we follow an electron in the longitudinal field F_x until it undergoes an intervalley scattering, at which point it is lost to

the simulation. The total time spent tracking that electron is saved and a new electron is started with the same initial conditions. This procedure is repeated until we have accumulated at least 400 000 scattering events and at least 1000 intervalley scatterings. The electron lifetime in the quantum wire is then obtained by averaging the time required to undergo intervalley scattering.

V. RESULTS

We have run Monte Carlo simulations at 300 and 77 K for two different confinement conditions. The first is a high-confinement condition characterized by $L_y = 135$ Å and $F_z = 120$ kV/cm. This condition places the bottom subband 138 meV above the quantum-well bottom and the first excited state 231 meV above the well bottom. The second case is a lower-confinement condition with $L_y = 215$ Å and $F_z = 20$ kV/cm, which places the bottom two levels 45 and 73 meV above the well bottom, respectively.

We have varied the electron initial energy as well as the electron initial subband; we find only a small dependence of the electron lifetime on the energy and essentially no dependence on the initial subband. The lack of dependence on initial subband can be explained by noting that the intervalley scattering rate in Fig. 2 is the same for both subbands *a* and *b*.

In Fig. 3, we present the electron lifetime in the high-confinement case as a function of initial energy for two different longitudinal fields. The temperature is 300 K, curve *a* shows the carrier lifetime in the presence of a longitudinal field of 1000 V/cm, and curve *b* is for a lower field of 100 V/cm. The lifetime is relatively independent of the inital energy for energies near the subband bottom and is about 150 ps at 100 V/cm and 50 ps at 1000 V/cm. Although the actual value of the lifetime at low energy depends on temperature, field, and confinement conditions, the different curves are all approximately parallel. At higher initial energies, the lifetime decreases at the threshold for intervalley scattering which occurs at 262 meV for phonon absorption to the *L* valley. At high longitudinal fields, the transition is smoother, but still occurs at roughly the same initial energy. The existence of two distinct energy regions in the curves can be understood as a trade-off between the intervalley-scattering time and the time required to reach equilibrium. We would expect the time required to scatter intervalley to be proportional to $\exp[-(E-E_t)/kT]$, where E_t is the threshold energy for intervalley scattering and E is some characteristic energy of the system. Normally, E is the initial energy, however, if the time is longer than that required to reach equilibrium, the system reaches equilibrium before undergoing an intervalley scattering and the time is independent of the initial energy.

In Fig. 4 we show the influence of the longitudinal field on the time and distance required to undergo an intervalley scattering event. The inset in Fig. 4 shows an estimate of the distance an electron travels for *a*, high, and *b*, low, confinement at 300 K. The high-confinement curves are for a simulation where the initial electron energy is 140 meV while in the low-confinement case the initial electron energy is 50 meV. Varying the initial energy does not substantially alter the result except for very high initial energies (as can be expected from Fig. 3). These distances are only approximations as they are calculated assuming $\langle x \rangle = \langle v \rangle \langle t \rangle$ rather than explicitly calculating $\langle x \rangle = \langle vt \rangle$ where x is the distance, v is the velocity, and t is the lifetime (the reason lies in the Monte Carlo code which keeps statistics on velocity and time independently and does not keep track of correlations between the two). This assumption limits the validity of the results to long lifetimes where the velocity is sufficiently randomized and electron runaway is not important. Accordingly, we do not present the distance for the 77-K case, or for longitudinal fields larger than 2 kV/cm (al-

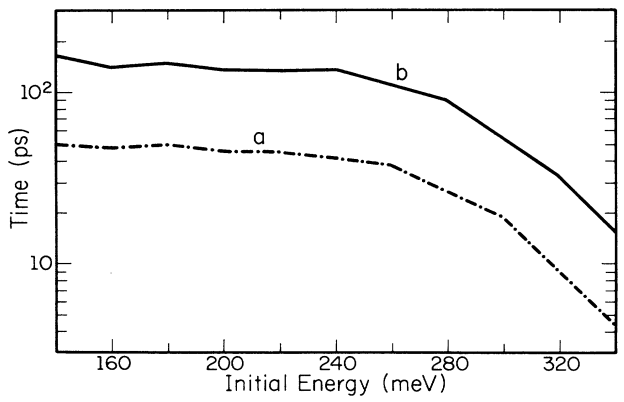

FIG. 3. Electron lifetime in quantum wires as a function of initial energy for two different longitudinal fields under high-confinement conditions at $T = 300$ K. *a* is for a longitudinal field of 100 V/cm, while *b* is for a longitudinal field of 1000 V/cm.

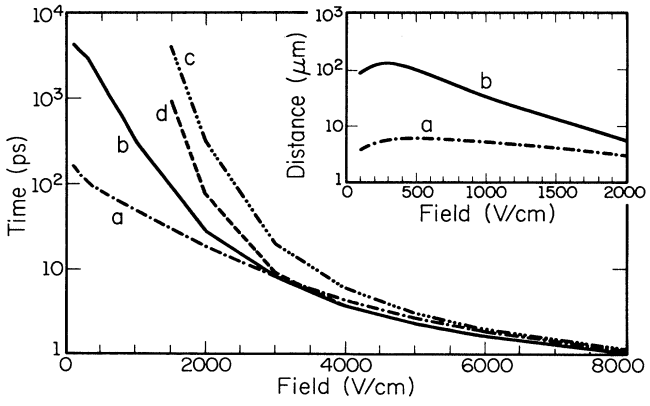

FIG. 4. Electron lifetime and distance vs longitudinal field at 77 and 300 K for high- and low-confinement conditions. *a* and *b* are high and low confinement at 300 K, respectively, while *c* and *d* are the corresponding curves for 77 K. Assumptions used in calculating the distance limit its validity to 300 K and fields below 2 kV/cm.

though the trend is clearly to shorter distances as the field increases). The distance in the low-confinement case is much larger than that for the high-confinement case, even though electron velocities in high confinement are larger than in low confinement. The distance rises rapidly, peaks near 400 V/cm, and then drops off slowly. This behavior can be understood by considering the two extremes of infinite and zero field. At very large fields, the lifetime is so short that even though the acceleration is very high, the distance still tends towards zero. At zero field, electrons still scatter by intervalley phonons with some small, but finite probability. Since the average velocity is zero, the average distance, as previously defined, required to undergo an intervalley scattering is zero. Of course, a more meaningful concept for the zero-field case would be $\langle d \rangle = \langle v_{\rm th} t \rangle$, where $v_{\rm th}$ is the thermal velocity. We estimate this to be approximately 44 μm under high confinement and 1150 μm for low confinement. These numbers are larger than one would estimate from extrapolation in the figure; however, $v_{\rm th}$ is considerably larger than the average (drift) velocity at low field and the results would converge at higher fields.

The influence of the longitudinal field on the lifetime is shown in Fig. 4 for high and low confinement at both 77 and 300 K. Curve $a(b)$ is for high (low) confinement at 300 K; $c(d)$ is high (low) confinement at 77 K. All curves show a very strong dependence on the longitudinal field. At lower fields, the effects of confinement and temperature are significant, but at higher fields these effects are washed out as the field dominates in determining the lifetime. The times (for the same field) are larger at 77 K because of the lack of phonon absorption, which tends to both lower the average energy and also raise the threshold for intervalley scattering. The 77-K results do not go below 1500 V/cm because the lifetime is over 10 ns and it requires too much CPU time to get an accurate estimate of the lifetime.

The fraction of electrons above the scattering threshold for the four different cases is tabulated in Table I and supports the data in Fig. 4. The cases with shorter lifetimes have greater carrier concentrations above the threshold for intervalley scattering. As can be seen, the high-confinement condition at 300 K has a much shorter lifetime than the low-confinement case. This is due to the fact that under high confinement the average energy is high because of the location of the bottom subband relative to the L or X valley. However, at 77 K the trend is reversed and under low confinement a larger fraction of carriers is above the emission threshold.

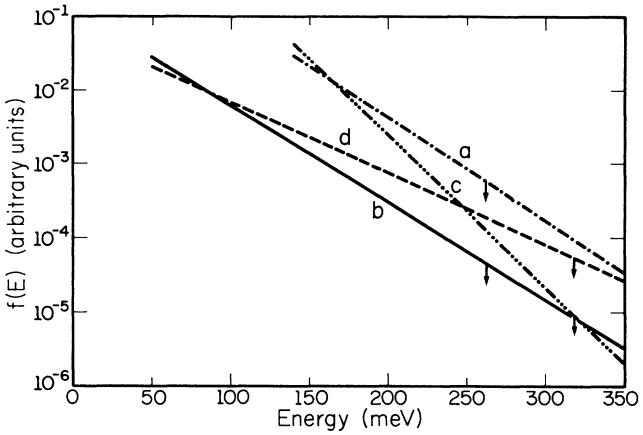

FIG. 5. Idealized distribution functions for the four cases shown in Fig. 4. The 300-K curves, a and b, are for a longitudinal field of 500 V/cm while the 77-K curves, c and d, are for a longitudinal field of 1500 V/cm.

Figure 5 presents a highly schematic picture of the distribution functions for the four cases. If we compare the two distribution functions at 300 K (a and b), it is apparent that the field does not play a major role since in both cases the high-energy slope of the distribution function is characterized by an electron temperature of approximately 400 K. Near equilibrium, detailed balance requires the distribution function to be insensitive to the confinement. However, at 77 K, hot carriers are much more important due to the lower lattice temperature and the higher longitudinal field. The corresponding electron temperatures are 260 K for the high-confinement case (c) and 550 K for the low confinement case (d). Therefore we suspect this difference is due to the dependence of the scattering rates on confinement and energy. At high fields, detailed balance is irrelevant and consequently the tail of the distribution function is more sensitive to the scattering rate. At high energy, where carriers undergo intervalley transfer, the effective POP scattering rate is stronger under high confinement than under low confinement due to the overlap integral in the matrix element.[15] As a result, the tail of the distribution function decreases more rapidly in the former case than in the latter, resulting in lower electron temperatures. This high-field effect results in longer electron lifetimes for the high-confinement case and can be seen at 300 K for fields above 3 kV/cm where curves (a) and (b) cross over.

TABLE I. Simulation conditions for the four cases shown in Figs. 4 and 5. The fraction is the fraction of carriers found above the threshold for intervalley scattering (262 meV at 300 K and 318 meV at 77 K) and the time is the average electron lifetime.

Case	Confinement	Temperature (K)	Field (V/cm)	Fraction %	Time (ps)
a	High	300	500	0.679	84
b	Low	300	500	0.0338	1580
c	High	77	1500	0.00523	3985
d	Low	77	1500	0.0602	926

VI. CONCLUSIONS

In conclusion, we have performed the first multisubband quasi-1D simulation which includes intervalley scattering to 3D states. The electron lifetime and distance for escaping the wire are not only very strong functions of longitudinal field but also are dependent on the confinement conditions and temperature. Lifetimes ranging from 4 n down to 1 ps have been calculated at 77 and 300 K for two confinement conditions with distances ranging from 130 μm down to the submicrometer range. The computed distances are in the 10-μm range for fields below 2 kV/cm at 300 K, which demonstrates the feasibility of operating quantum wires as purely 1D structures without being concerned with intervalley scattering. On the other hand, under high-field conditions, electrons escape the wire quickly. This should be accompanied by a corresponding negative differential resistance in the I-V characteristics similar to real space transfer as they scatters from high mobility 1D states in the Γ valley to lower mobility 3D states in the L or X valleys.

ACKNOWLEDGMENTS

The authors are indebted to Karl Hess for helpful discussions on real-space transfer. This work is supported by National Science Foundation Grant No. NSF-CDR-85-10209 and the Joint Services Electronics Program.

[1]H. Sakaki, Jpn. J. Appl. Phys. **19**, L735 (1980).
[2]P. Petroff, A. Gossard, R. Logan, and W. Wiegmann, Appl. Phys. Lett. **41**, 635 (1982).
[3]A. Warren, D. Antoniadis, and H. Smith, Phys. Rev. Lett. **56**, 1858 (1986).
[4]K. Kash, A. Scherer, J. Worlock, H. Craighead, and M. Tamargo, Appl. Phys. Lett. **49**, 1043 (1986).
[5]T. Hiramoto, K. Hirakawa, Y. Iye, and T. Ikoma, Appl. Phys. Lett. **51**, 1620 (1987).
[6]M. L. Roukes, A. Scherer, S. J. Allen, H. G. Craighead, R. M. Ruthen, E. D. Beebe, and J. P. Harbison, Phys. Rev. Lett. **59**, 3011 (1987).
[7]K. Ismail, D. A. Antoniadis, and H.I. Smith, Appl. Phys. Lett. **54**, 1130 (1989).
[8]M. Tsuchiya, J. M. Gaines, R. H. Yan, R. J. Simes, P. O. Holtz, L. A. Coldren, and P. M. Petroff, Phys. Rev. Lett. **62**, 466 (1989).
[9]E. Kapon, D. M. Hwang, and R. Bhat, Phys. Rev. Lett. **63**, 430 (1989).
[10]S. Briggs and J. P. Leburton, Phys. Rev. B **39**, 8025 (1989).
[11]J. P. Leburton, J. Appl. Phys. **56**, 2850 (1984).
[12]G. Fishman, Phys. Rev. B **34**, 2394 (1986).
[13]S. Laux and F. Stern, Appl. Phys. Lett. **49**, 91 (1986).
[14]J. Lee and H. Spector, J. Appl. Phys. **57**, 366 (1985).
[15]S. Briggs and J. P. Leburton, Phys. Rev. B **38**, 8163 (1988). In this reference, Eq. (4) should be corrected to agree with Eq. (8) in this paper.
[16]S. Das Sarma and X. C. Xie, Phys. Rev. B **35**, 9875 (1987).
[17]A. Kubasi, C. Chattopadhyay, and C. K. Sarkar, J. Appl. Phys. **65**, 1598 (1989).
[18]K. Hess, H. Morkoc, H. Shichijo, and B. G. Streetman, Appl. Phys. Lett. **35**, 469 (1979).
[19]E. O. Kane, J. Phys. Chem. Solids **1**, 249 (1957).
[20]E. M. Conwell, *High Field Transport In Semiconductors* (Academic, New York, 1967).
[21]W. Fawcett, A. D. Boardman, and S. Swain, J. Phys. Chem. Solids **31**, 1963 (1970).
[22]N. Mori and T. Ando, Phys. Rev. B **40**, 6175 (1989).
[23]S. Briggs, B. A. Mason, and J. P. Leburton, Phys. Rev. B **40**, 12 001 (1989).
[24]C. Jacoboni and L. Reggiani, Rev. Mod. Phys. **55**, 645 (1983).
[25]R. Yortson, J. Comput. Phys. **64**, 177 (1986).